Robust and accurate decoding of motoneuron behavior and prediction of the resulting force output

Christopher K. Thompson[1]*, Francesco Negro[2]*, Michael D. Johnson[3], Matthew R. Holmes[3], Laura Miller McPherson[4], Randall K. Powers[5], Dario Farina[6#], Charles J. Heckman[3#]

[1]Department of Physical Therapy, Temple University
[2]Department of Clinical and Experimental Sciences, Università degli Studi di Brescia
[3]Department of Physiology, Northwestern University
[4]Department of Physical Therapy, Florida International University
[5]Department of Physiology and Biophysics, University of Washington
[6]Department of Bioengineering, Imperial College London

* Contributed equally to the analysis and experimental work for this study
# Contributed equally to the planning and coordination of the study

Running title: Neural drive to muscle and resulting force output

Key Words: motor unit, muscle, decomposition, high-density EMG, cat model

Section: Techniques in Physiology

Table of Contents Category: Neuroscience – cellular/molecular

Number of figures/tables: 6/0

Corresponding authors:
Charles (CJ) Heckman, PhD
303 E Chicago Avenue, Room 5-334
Chicago IL 60611
c-heckman@northwestern.edu
+1 (312) 503 2164

Dario Farina, PhD
SW7 2AZ London, UK
d.farina@imperial.ac.uk
+44 (0) 20 759 41387

Key Points Summary

- The spinal alpha motoneuron is the only cell in the human CNS whose discharge can be routinely recorded in humans.
- We have reengineered motor unit collection and decomposition approaches, originally developed in humans, to measure the neural drive to muscle and estimate muscle force generation in the decerebrate cat model.
- Experimental, computational, and predictive approaches are used to demonstrate the validity of this approach across a wide range of modes to activate the motor pool.
- The utility of this approach is shown through the ability to track individual motor units across trials, allowing for better predictions of muscle force than the electromyography signal, and providing insights in to the stereotypical discharge characteristics in response to synaptic activation of the motor pool.
- This approach now allows for a direct link between the intracellular data of single motoneurons, the discharge properties of motoneuron populations, and muscle force generation in the same preparation.

Abstract

The discharge of a spinal alpha motoneuron and the resulting contraction of its muscle fibers represents the functional quantum of the motor system. Recent advances in the recording and decomposition of the electromyographic signal allows for the identification of several tens of concurrently active motor units. These detailed population data provide the potential to achieve deep insights into the synaptic organization of motor commands. Yet most of our understanding of the synaptic input to motoneurons is derived from intracellular recordings in animal preparations. Thus, it is necessary to extend the new electrode and decomposition methods to recording of motor unit populations in these same preparations. To achieve this goal, we use high-density electrode arrays and decomposition techniques, analogous to those developed for humans, to record and decompose the activity of tens of concurrently active motor units in a hindlimb muscle in the decerebrate cat. Our results showed that the decomposition method in this animal preparation was highly accurate, with conventional two-source validation providing rates of agreement equal to or superior to those found in humans. Multidimensional reconstruction of the motor unit action potential provides the ability to accurately track the same motor unit across multiple contractions. Additionally, correlational analyses demonstrate that the composite spike train provides better estimates of whole muscle force than conventional estimates obtained from the electromyographic signal. Lastly, stark differences are observed between the modes of activation, in particular tendon vibration produced quantal interspike intervals at integer multiples of the vibration period.

Abbreviation list

BSS, blind source separation; CST, composite spike train; EMG, electromyography; MUAP, motor unit action potential; ISI, interspike interval; RoA, rate of agreement; STA, spike triggered average

Introduction

The functional quantum of the motor system is the motor unit, which consists of a single spinal alpha motoneuron and the muscle fibers it innervates (Heckman & Enoka, 2012). The neuromuscular junction has a large safety factor in synaptic transmission (Wood & Slater, 2001) resulting in a one-to-one relation between the discharge of a motoneuron and the activation of its muscle fibers. Because each motoneuron innervates a relatively large number of muscle fibers, their discharge patterns provide a highly amplified version of the discharge pattern of their parent motoneuron. Because of this, the spinal motoneuron is the only CNS cell whose firing pattern can be routinely recorded in humans, providing a wealth of information about the structure of motor output.

Motor unit recordings have historically been obtained through needle or fine wire techniques (Adrian & Bronk, 1929). Subsequently, semi-automated threshold and template matching algorithms have been developed to decompose these intramuscular electromyographic (EMG) signals into the discharge times of individual motor units (De Luca *et al.*, 1982; Stashuk, 1999; McGill *et al.*, 2004; Parsaei *et al.*, 2010). However, this invasive approach can only provide selective EMG recordings from a relatively small number of motor units per contraction (Duchateau & Enoka, 2011). Recent development of surface and intramuscular array electrodes and automated decomposition algorithms now allows for the quantification of the discharge of several tens of concurrently active motor units in humans (Holobar *et al.*, 2010; Nawab *et al.*, 2010; Farina & Holobar, 2016; Negro *et al.*, 2016).

The population behavior of motor units has the potential to reveal much about the synaptic control and intrinsic properties of motoneurons (Collins *et al.*, 2002; Farina & Negro, 2015; Muceli *et al.*, 2015). The interpretation of the behavior of motor unit populations is aided by a wealth of data that has been obtained from intracellular recordings of synaptic inputs and motoneuron properties in a variety of reduced animal preparations (Heckman & Enoka, 2012; Johnson *et al.*, 2017). Ultimately, the relationship between the intracellular data of single motoneurons, the discharge of motoneuron populations, and muscle force generation can be revealed by comparing these data sets in the same preparation.

To this end, our goal was to adapt an EMG array recording technique, originally developed in humans, to record motor unit populations and muscle force generation in the cat to demonstrate the validity and utility of this approach. This approach allowed for the accurate decomposition of several tens of concurrently active motor units during contractions of the soleus muscle. Using two-source validation, we found the accuracy of the motor unit decomposition to be comparable to, or better than, those obtained in human muscles. Further, reconstruction of the motor unit action potential (MUAP) allows us to further validate the technique and track the same motor unit across multiple contractions. The utility of these approaches is demonstrated by showing that a filtered version of the composite motor unit spike train (CST) was a better predictor of muscle force as compared to the filtered, rectified EMG, particularly for

the higher frequencies of muscle force generation. Lastly, we have demonstrated a quantal discharge pattern in response to homonymous tendon vibration and the preferred discharge of individual motor units across vibration frequencies.

Methods

Ethical approval

Data presented here are from 15 adult cats of either sex. All animals were obtained from a designated breeding establishment for scientific research. Animals were housed at Northwestern University's Center for Comparative Medicine, an AAALAC accredited animal research program. All procedures were approved by the Institutional Animal Care and Use Committee at Northwestern University and conform to the ethics policy of the Journal of Physiology (Grundy, 2015).

Terminal surgery

Anesthesia was induced with 4% isoflurane and a 1:3 mixture of N_2O and O_2. The depth of anesthesia was monitored through continuous monitoring of blood pressure, heart and respiratory rate, and absence of withdrawal reflexes throughout surgery. A tracheostomy was performed and a permanent tracheal tube was placed though which isoflurane (0.5 – 2.5%) and gasses were delivered for the duration of the surgical procedures. The animal was then transferred to a stereotaxic frame and immobilized by a head clamp, spinal clamp on the L2 dorsal vertebral process, and bilateral hip pins at the iliac crest. The left hindlimb was immobilized through pins at the knee and clamps at the ankle, and the right hindlimb was secured using a clamp at the lower leg. The left soleus was dissected, isolated, and its distal tendon was attached to a load cell via a calcaneus bone chip in series with a linear variable differential transformer and customized voice coil. A distal, cutaneous branch of the right superficial peroneal nerve was surgically dissected and a cuff electrode was secured around the nerve. On select experiments, a L4-S1 laminectomy was provided for intrathecal drug administration via subdural catheter. The dorsal and ventral roots were left intact. In all experiments, following a craniotomy, a precollicular decerebration was performed. At this point the animals are considered to have a complete lack of sentience and anesthesia was discontinued (Silverman *et al.*, 2005). A thermistor was placed in the esophagus and core temperature was maintained at 35-37^{o}C using heat lamps and hot pads throughout the experiment. At the end of the experiment animals were euthanized using a 2 mM/kg solution of KCl in addition to a bilateral thoracotomy.

Data collection

Referenced monopolar EMG recordings were collected using a custom 64-channel array electrode placed on the surface of the exposed soleus muscle. The array consisted of 64 individual rigid silver pins, 7.5 mm in length and 0.7 mm in diameter, configured in a 5 x 13 matrix with an interelectrode distance of 2.54 mm. A ground electrode was place on the back and a reference electrode was placed on the upper thigh. Array data were filtered (100 – 900 Hz), amplified (0.5 – 2k) and sampled at 5120 Hz by a 12-bit

A/D converter simultaneously with soleus force data (EMG-USB 2, 256-channel EMG amplifier, OT Bioelettronica, Torino, Italy).

Additionally, up to three pairs of perpendicularly cut, barbed, 75 μm stainless-steel fine wires (A-M Systems, Carlsborg, WA) were inserted into the soleus via a 23-gauge needle. Fine wire signals were each filtered (0.01 – 3.0kHz) and amplified (1 – 10k) using separate floating differential amplifiers (DAM50, World Precision Instruments, Sarasota, FL) and collected at 20 kHz simultaneously with the force data (1401, Cambridge Electronic Devices, Cambridge, ENG).

EMG and force from the left soleus muscle were recorded during four modes of activation. First, spontaneous, repetitive discharge of motor units is often observed in the decerebrate cat. This is defined here as any motor output remaining more than 5 seconds following the cessation of a specific input. Second, tendon vibration was delivered at high frequencies (~130 Hz) and small amplitude (~80 μm) through the voice coil. This provides potent and selective activation of Ia afferents (Brown *et al.*, 1967) and activates the homonymous motoneuron pool through monosynaptic pathways. Third, excitation of the soleus can be reliably evoked through the crossed extension reflex elicited via electrical stimulation of contralateral nerves. Here 1-ms stimulus pulses were delivered to the contralateral superficial peroneal nerve through the cuff electrode using a Grass S88 stimulator and isolation unit. Stimulation was delivered at either a constant frequency or a linearly increasing and decreasing frequency stimulation pattern in the range of 10 to 50 Hz. Fourth, a 2-5 mm ramp and hold stretch at 0.5-2 mm/s of the soleus muscle activates muscle receptors resulting in homonymous excitation through mono- and polysynaptic pathways (Jankowska *et al.*, 1981). Lastly, to increase the activity of soleus motoneurons, during select experiments, 25 – 100 uL of 100 mM Methoxamine, a norepinephrine α1 agonist, was applied to the spinal cord through the intrathecal catheter. Methoxamine has been shown previously to increase the excitability of spinal motoneurons through increased magnitude of persistent inward currents (Lee & Heckman, 1999).

Motor unit decomposition

Offline, each array recording was visually inspected and up to 64 acceptable monopolar channels were isolated for further processing. EMG data collected from the array were decomposed into their corresponding motor unit action potentials using a custom implementation of the blind source separation approach for multi-channel EMG signals previously used in human studies (Holobar *et al.*, 2010; Negro *et al.*, 2016). Briefly, the procedure of identifying the sources (i.e. motoneuron spike trains) and the mixture matrix that are generating a recorded multichannel signal is called blind source separation (BSS). In the case of EMG signals, the mixture is convolutive, with various weights and delays in sources. For this reason, convolutive BSS methods are applied. In particular, the recorded multichannel signals are

first extended to transform the convolutive problem into an instantaneous one. This procedure aims to compensate for the delays in the original signals. After this pre-processing step, the instantaneous model can be sphered (spatial-temporal whitened) and inverted using optimization methods that maximize appropriate statistical measures of the sources in order to estimate the original mixing weights. In the case of the relatively low frequency of motoneuron discharge, the sources generate a naturally sparse distribution of discharges. For this reason, optimization methods that maximize measures of sparsity and non-gaussianity are applied to decompose the multi-channel EMG signals (Farina & Holobar, 2016). In practice, the algorithms find solutions to the inverse problem that are far from Gaussianity and have high kurtosis. In this study, this procedure was applied following the steps previously presented (Holobar *et al.*, 2010; Negro *et al.*, 2016) with a selection of parameters (extension factor of the measures equal to 10, number of removed principal components equal to 25%) suitable for the higher selectivity of the cat EMG signals compared with the human recordings. Only sources with a silhouette (or pulse to noise ratio) measure higher than 0.9 (30 dB) were used for subsequent data analysis (Holobar *et al.*, 2014; Negro *et al.*, 2016).

Fine wire recordings were decomposed into corresponding motor units using the open source EMGLab software (McGill *et al.*, 2005). Offline, recordings were high-pass filtered (typically 1 kHz), a template matching algorithm was employed to automatically create templates, classify individual motor unit action potentials, and provide the residual signal using a sliding window of 5 to 10 seconds. This resulting decomposition was manually inspected and corrected as necessary. Following decomposition of the segment, the window was moved ~4s ahead and the process was repeated until full decomposition was achieved. Discharge times for each unit were exported at 1000 Hz for further processing.

Data analysis

Various approaches have been used to quantify the accuracy of a decomposed motor unit spike train (Farina *et al.*, 2014). The most stringent method remains to record and decompose the discharge of a single motor unit using two separate approaches simultaneously (Mambrito & De Luca, 1984) and compare the results. We assessed the correspondence between motor unit discharge times obtained from the fine wire and multi-channel EMG signals using the rate of agreement (RoA), defined by the following equation:

$$\mathrm{RoA} = \frac{D_C}{D_C + D_A + D_W} * 100$$

Here, D_C equals the number of discharges common to both the array and the wire within 0.5 ms of one another. D_A equals the number of discharges identified just by the array recording. D_W equals the number

of discharges identified just by the wire recording. This approach treats each discharge equally, regardless of the source, and provides a normalized value, where 100 is a perfect correspondence between sources.

The combined signals of the 64 channels of the array provide a unique spatiotemporal view of the motor unit action potential (MUAP) waveform of a given motor unit. The MUAP was revealed through spike triggered averaging (STA) the motor unit action potential trains with greater than 50 discharges into each of the 64 channels across a 35 ms window centered on the decomposed spike time. These data were interpolated across the known interelectrode distance to calculate the multidimensional spatiotemporal MUAP waveform. The MUAP waveforms can provide a unique voltage signature for each of the decomposed motor units throughout time, which can readily be observed through visual estimation. The uniqueness of the MUAP can be quantified by calculating the 2D crosscorrelation of a given MUAP waveform with all other waveforms in a given trial (Cescon & Gazzoni, 2010; Gligorijevic *et al.*, 2015; Martinez-Valdes *et al.*, 2016). Moreover, this waveform correlation approach allows us to track motor unit discharge patterns across trials by quantifying waveform similarity. In general, the probability of different motor units showing the same spatial MUAP representation decreases considerably with the number of recording channels (Farina *et al.*, 2008). Here, MUAP waveforms, extracted from up to 64 monopolar signals, were considered the same if they demonstrated a normalized correlation value greater than 0.85.

In addition to correlations within and across trials, the MUAP waveform contains information about both the biophysical characteristics of the motor unit and its distance from the recording source. The peak-to-peak amplitude of the MUAP across the entire array can be extracted and may provide indirect information about the size of the motor unit (McPherson *et al.*, 2016). Additionally, these measures allow us to assess muscle fiber conduction velocity. Motor unit conduction velocity was estimated using a previously validated method (Farina *et al.*, 2001). For the calculation, only the largest set of channels (four or five) that showed stability in the shapes of the MUAP were selected (correlation > 0.9 between channels) in each trial. Obtaining similar waveform measurements across multiple trials supports the notion that the same motor unit is indeed being detected (Martinez-Valdes *et al.*, 2016).

Estimation of force generation was accomplished using both the EMG signal and the decomposed motor unit spike times. For each recording, one subset of five reliable EMG channels from the 64-channel array were randomly selected for the analysis. For each of these channels, an optimization routine was used to maximize the correlation between the force and EMG signals. For each trial, the force signal was baseline corrected, low-pass filtered using a 2-pole, zero phase lag, 10 Hz Butterworth filter, and normalized by dividing by the maximum of the signal. Each EMG channel was full-wave rectified and filtered using a 3rd order Butterworth filter; the cutoff of the filter was optimized to from 0.1 to 5 Hz in 0.05 Hz steps while the scaling of the EMG was optimized from 0.1 to 100 in 0.05 steps. Following each

permutation, the linear correlation between the force and EMG was calculated. The maximum correlation across all permutations was determined.

A similar approach to force estimation was conducted using the decomposed motor unit spike times. Here the spike times were converted into a continuous binary signal and the cumulative spike train (CST) was constructed by summing these individual binary spike trains across motor units. This provided an estimate of the neural drive to muscle. Force was estimated by convolving the CST with the impulse response of a critically dampened, second-order system f(t), which has been used extensively to model the motor unit twitch force (Fuglevand *et al.*, 1993):

$$f(t)= \frac{P \cdot t}{T} \cdot e^{1-(\frac{t}{T})}$$

Using this equation, a brute force optimization procedure was used to optimally scale both P, the peak twitch force, from 0.01 to 0.11 in 0.001 steps, and T, the rate of force development, from 30 to 300 ms in 0.1 ms steps. A similar approach of maximizing the correlation between the force and spike trains was conducted.

The spike train data allowed us to assess how many motor units are necessary to accurately recreate force output. This was accomplished by iteratively increasing the number of motor units used in the composite spike train, from 1 to the total decomposed units in each trial. The force and spike train correlation was re-optimized for each increase in spike train number.

To quantify the ability of the EMG and CST to estimate the higher frequency component of muscle force, these signals were re-optimized in a similar manner, except, just prior to optimization, the torque, EMG, and CST signals were high pass filtered at 0.75 Hz using a 2^{nd} order, zero-lag, Butterworth filter. Then these filtered signals are optimized using a similar routine as above.

A one-way repeated-measures analysis of variance (ANOVA) was used to assess changes in the uniqueness of motor unit action potential waveforms, corrupted by various amounts of noise and differences in force estimation across the EMG and CST signals. When significant, a post-hoc Tukey Honestly Significant Difference was used to assess the significance of pairwise comparisons.

Results

Rate of agreement with fine wire signals

A representative multi-channel EMG recording is shown in Figure 1. Validation of the decomposition of motor units can be accomplished through comparing the spike times found using the array decomposition to those derived from traditional fine wire approaches. Figure 2 shows an example trial during spontaneous discharge, where three of the 12 spike trains decomposed from the multi-channel EMG array matched spike trains recorded by the fine wires, and the rate of agreement (RoA) varied from 97.8 to 100%. In 49 trials from 11 experiments, we were able to find 201 motor unit spike trains common to both the array and fine wire approaches. Across these 201 units, an average RoA of 93.3 ± 8.2% was observed. The form of input had a significant impact on the rate of agreement. Spontaneous discharge demonstrated the highest RoA at 98.0±2.6%, followed by crossed extension (95.8 ± 5.3%) and tendon vibration (92.7 ± 7.7%). Stretch demonstrated the least reliable 2-source validation with a RoA of 86.0 ± 11.4%.

Outside of the form of input, other factors may influence the detection of a MUAP. For example, it may be more difficult for the decomposition algorithm to detect units of smaller amplitude. To assess this, the peak-to-peak amplitude was calculated for the MUAP extracted from each spike train and correlated with the RoA value. Such correlation was practically nonexistent, with an r^2 value less than 0.001. Therefore, the average amplitude of the MUAPs is not a factor that can influence the convergence of the algorithm on reliable solutions. However, with the exception of one spike train, motor units with a MUAP amplitude >0.85 mA demonstrate RoA values greater than 90%. Additionally, it might be the case that the number of units detected may influence the accuracy of the decomposition. It is conceivable that the greater number of motor units detected for a given trial, the more likely it may be for mistakes to occur. Though the relationship was relatively weak ($r^2 = 0.049$), we found the opposite result; a significant ($p<0.001$) positive correlation is observed between the number of units collected on a given trial and the RoA values. Lastly, the number of discharges detected for a given motor unit spike train was strongly correlated with RoA. With the exception of three spike trains, all of the spike trains that detected 50 or more spikes had RoA values greater than 90%. This relationship is best described by a 2-term power function with an r^2 value of 0.96. Therefore, when the algorithm can converge well in multiple local maxima, it will likely extract many reliable units. Similarly, good solutions should have more spikes compared to solutions with lower number of discharges.

Reconstruction of the MUAP waveform

Through STA approaches, we are able to create 64 unique views of the MUAP of each motor unit and reconstruct the spatiotemporal dynamics of the MUAP waveform. Figure 3 shows two motor unit action potential waveforms. The unique representation of each waveform can be visually appreciated and

calculated by 2D cross correlation across all of the resulting MUAP waveforms within a given trial. The correlation matrix in Figure 3B demonstrates that any given MUAP waveform rarely correlates with other MUAP waveforms. A measure of uniqueness of a given unit can be provided by calculating the average correlation of this unit with all other units collected and subtracting this from the correlation of this unit with itself (1 in the absence of noise, see below). The MUAP waveform shapes derived from the STA are consistent with the physiology underlying the motor unit action potential. However, it is possible for seemingly valid MUAP waveforms to be constructed from trigger events not necessarily corresponding to motor unit discharges (Farina *et al.*, 2014). To control for this possibility, Figure 3 demonstrates that the uniqueness in MUAP waveforms is disrupted by adding variability to the discharge times. To test the effects of variability in spike detection, an increasing amount of random Gaussian noise was added to the discharge times, ranging from 1% to 20% of the standard deviation of the interspike interval (ISI). Thus, we are comparing a given trial with itself, each of which is corrupted by small amounts of different noise. In the 13 units decomposed in this example, as little as 5% corruption significantly diminished the uniqueness of any given unit from the other concurrently active units. This test is different from that proposed by Hu *et al.* (2013), which analyzed the amplitude of the individual MUAP waveforms extracted by STA, rather than the similarity across two dimensional MUAP waveforms, when introducing a similar variability in the discharge times.

Further validation is provided by matching the individual MUAP waveforms across separate trials. This relies on the assumption that it is extremely unlikely that triggers not associated with true motor unit discharges would produce highly correlated MUAP waveforms on two separate trials. Figure 4 demonstrates the stability of the MUAP waveform across trials, for three motor units recorded across 7, 4 and 10 trials. Although there are small variations in peak-to-peak amplitude and conduction velocity across trials, the value of the 2D cross-correlation remained high (>85%).

Though we are able to track units, we are not able to track all of the units across all of the contractions. This could be due to physiological rotation of motor units across trials and/or limitations in our ability to collect and process the signal. For example, slight changes in the position of the electrode make cumulative changes the derived MUAP waveform over time. If this were the case, one would expect to see adjacent trials match to a higher extent than trials performed several minutes later. To assess this possibility, the number of matches between the first trial to the subsequent nine demonstrated no apparent role of trial order in the number of motor units matched, nor did order matter when the tenth trial is compared with the previous nine. Further, it is possible that larger amplitude waveforms are relatively easier to detect, and therefore smaller waveforms may be less frequently matched across trials. If this were the case, one would expect larger units to be detected as common more frequently than smaller

waveforms. This was not observed in the current data, as no correlation between the size of the MUAP and the number of trials was detected.

Estimation of muscle force

Estimation of muscle force through the muscle's electrical activity was performed on a pool of 188 trials from seven experiments; 22 trials contained spontaneous discharge, 24 trials contained responses to tendon vibration, and 140 trials contained responses to crossed extension. For each of the trials, five acceptable EMG channels were chosen at random, rectified, and optimally scaled and filtered to fit the force record by maximizing the correlation between the force and the processed EMG signals (Figure 5a). On average, channels chosen at random could fit the force with the mean correlation across the five channels of 92.6±0.6. Across the five EMG fits, average correlation values ranged between 92.2±0.8 to 92.9±0.8 with no significant difference across channels ($p=0.657$).

A similar approach was applied to the CST by convolving the CST with a motor unit twitch force model whose amplitude and time to peak were optimized (Figure 5b). The CST provided a strong estimate of the overall force output, with the average fit being 96.3±0.03. The optimal fit provided by the CST produced greater correlations than each of the 5 random rectified interference EMG recordings ($p<0.0001$; Figure 5c). Although the average correlation with force was high for both analyses, the type of input had a significant effect on the estimation of muscle force. For the spontaneous discharge, the EMG based estimate of force (83.4±3.8) was substantially poorer ($p<0.0001$) than for the other conditions (crossed extension, 93.6±0.4, tendon vibration, 95.2±6.8). Conversely, the use of motor unit spike times was robust across conditions, with only a small decrease for the spontaneous discharge (94.7±1.1) as compared to the crossed extension (96.3±0.3) and tendon vibration (97.4±0.5; $p=0.046$). Across all conditions, the optimized rate of force development was found to be 138±65 ms, noticeably higher than the 80-100 ms rate of force development gathered from single soleus twitches (Burke, 1967; Lewis, 1972; Bagust, 1974; Burke et al., 1974), which may reflect differences in tendon compliance and muscle fiber contractions dynamics during sustained contractions versus single twitches.

The CST was able to better resolve higher frequency force fluctuations. To quantify this, we filtered the signals at 0.75 Hz and reassessed the optimization routine (Figure 5e-f). Across all conditions, the estimates of muscle force were worse. However, the CST continued to produce superior correlations with force (83.5±1.3) as compared to the EMG estimates (66.6±1.3; $p<0.0001$; Figure 5g).

Lastly, we were able to determine how many motor units are needed to accurately reproduce force generation by iteratively adding motor units in to the CST one-by-one and re-optimizing the force output. Figure 5d demonstrates that with only one motor unit spike train, optimal force estimation is rather poor, resulting in a correlation of only 77.7±25.0. With an increasing number of spike trains added to the CST,

the estimates improve. With nine or more motor units, the CST is a better prediction of force than the average EMG. In our sample of 188 trials, 179 trials contained the discharge pattern of at least nine motor units. For the trials with the greatest number of motor units (28), a correlation of 99.2±0.2 was observed, indicating almost perfect prediction of force from motor neuron behavior. Lower correlations were observed when the analysis was performed on the high-pass filtered data. With only one motor unit, the correlations with force were 57.4±1.8, however only three motor units were needed to produce superior correlations of high-pass filtered force as compared to the surface EMG (71.7±1.5 versus 66.6±0.7). When looking at the trials with only the greatest number of motor units, a correlation of 94.4±0.2 was observed with the high-pass filtered force.

Motor unit activation in response to tendon vibration

The particularly good fit of force estimation observed in response to tendon vibration was, at first, unexpected given the clear patterned motor unit discharge patterns observed in response tendon vibration. Figure 6 demonstrates motor unit discharge patterns evoked through response to tendon vibration. When the instantaneous discharge rate is plotted against time and superimposed, a clear banding of motor discharge rates is observed at integer multiples of the vibration period. These vibration-induced sub-harmonics in discharge patterns are clearly noted when the composite ISI histogram is constructed across the discharge for all units in a trial (Figure 6a). In contrast, the composite ISI histogram is relatively smooth for the tonic discharge input (Figure 2b), showing only two broad clusters of spike times. Such punctuated histograms were observed in every tendon vibration trial across every experiment. Figure 6a demonstrates the composite ISI histogram in response to ~130 Hz tendon vibration from six different experiments; each trial demonstrates this punctuated pattern. This quantal discharge pattern is consistently observed across a range of vibration frequencies (see inset with the waveforms in Figure 6b), with the magnitude of the quantal discharge proportional to the period of the vibration wave.

Though each motoneuron demonstrates this punctuated discharge, substantial variation is observed in the mean discharge of individual motoneurons. The lower panel in Figure 6b demonstrates this variation in motor unit responses to vibration. Though the population of motor unit discharge shows a relatively wide range of discharge, individual motor units are quite narrow in their range of discharge. Furthermore, when vibration is applied at various frequencies and motor units are tracked across these trials, each motor unit tends to maintain its "preferred" range of discharge frequency.

Discussion

In this study, we report the activity of tens of concurrently active motor units in the unanaesthetised, unparalyzed, decerebrate cat. This animal model has been used for 30+ years to investigate spinal physiology and neuromodulation of spinal neurons. Our EMG array approaches now provide similar information regarding the discharge of motoneuron populations in both animal and human models and will improve the fidelity of between-species comparisons.

Array methods in animal preparations as the link between system and cellular behaviors

Recording the activity of muscle has played a critical role in understanding the activation of spinal motoneurons. Adrian and Bronk (1929) were first to recorded the discharge of single muscle fibers, and did so in both in humans and in animals. This approach was refined with improved amplifiers, electrodes, and decomposition tools, but the underlying principle has remained a mainstay for nearly a century (Duchateau & Enoka, 2011; Farina *et al.*, 2016). The development of intracellular recording ushered in an era of intense investigation of the synaptic inputs and intrinsic electrical properties of motoneurons (reviewed in Stuart & Brownstone, 2011) resulting in a remarkably detailed understanding of the organization of synaptic input and intrinsic electrical properties of spinal motoneurons (reviewed in Powers & Binder, 2001; Heckman & Enoka, 2012). This knowledge base has allowed construction of highly realistic computer simulations of motoneurons (Powers *et al.*, 2012; Elbasiouny, 2014), which greatly aid in interpretation of motor unit firing patterns in humans (Johnson *et al.*, 2017).

Despite this progress, there exist two clear limitations. Motor unit recordings have been restricted to one or perhaps just few neurons at a time, limiting the insights about how motoneurons function as a population (Duchateau & Enoka, 2011). This limitation has largely been overcome by the array methods developed in humans (Holobar *et al.*, 2010; Nawab *et al.*, 2010; Farina & Holobar, 2016; Negro *et al.*, 2016). The second limitation is that, although the array recording methods were originally developed for human subjects, the understanding of the cellular mechanisms that generate the resulting population firing patterns depend on data obtained in intracellular recordings in motoneurons. These recordings can only be done in animal preparations, with most of these studies having been done in the cat preparation. Thus, our adaptation of the array methods for this preparation is uniquely valuable in that it allows array data, which captures the single neuron to population transition, to be recorded in the same preparation as intracellular data, which identifies cellular mechanisms. It is true that intracellular recordings in the decerebrate preparation usually require paralysis for recording stability, so simultaneous intracellular and muscle array recordings have not yet been attempted. Nonetheless, our results on tendon vibration illustrate the potential value of obtaining intracellular and array data in the same preparation.

The synaptic currents generated by tendon vibration in the medial gastrocnemius (MG) motoneurons have been extensively investigated and reveal strong amplification by persistent inward currents (PICs; Lee & Heckman, 1996; Hyngstrom *et al.*, 2008). The present array studies revealed two features of vibration induced inputs that have yet to be studied with intracellular methods. The banding in interspike interval due to the vibration frequency was not assessed in the intracellular studies, in which the current data was heavily filtered to focus on the contribution of PICs. It is not clear how these high frequency vibrations interact with the amplification induced by the PIC, which has a slow time constant (effectively about 50 ms; see Powers *et al.*, 2012; Powers & Heckman, 2017). The PIC may thus tend to damp vibration-induced oscillations so that without its effects, the banding seen in the present study might have been much stronger. The preferred firing range exhibited by each motor unit for these banded patterns may arise from differences in the recruitment threshold currents and spike afterhyperpolarizations (AHPs) that exist in every motor pool (Powers & Binder, 2001; Heckman & Enoka, 2012). Nonetheless the range of these differences is small in the cat soleus, which is almost 100% slow twitch (Burke, 1981). Finally, these vibration-induced discharge of motor units in soleus are low – ranging from about 5 to 10 Hz in the present. Although these intracellular studies in MG did not usually assess firing rates, much higher rates were observed in some cells (20 Hz and above; Lee & Heckman, 1996). As human motor units often fire at relatively low rates, intracellular studies of soleus motoneurons in the cat can be expected to reveal how low firing rates emerge and these banding patterns are created by the interactions of PICs, AHPs, and thresholds. The combination of intracellular recording and array recording in the cat thus has great potential for grounding system behavior in cellular mechanisms (see also the final section of this *Discussio*n).

Validation of motor unit recordings in the cat

Validation of motor unit discharge is necessary, though difficult, as there is no universally accepted gold standard (Farina *et al.*, 2014). A multitude of experimental, computational, and predictive approaches were used to evaluate the accuracy of the discharge times of individual motor units and to demonstrate the validity of this approach under a wide range of conditions.

The most stringent means to validate motor unit decomposition remains to record the same motor unit from two separate sources and to compare the discharge times (Mambrito & De Luca, 1984). Two-source validation assumes that coincident findings from two different methods of recording and processing are highly unlikely to occur. We observe RoA values that are equivalent to (Hu *et al.*, 2014) or slightly better (Yavuz *et al.*, 2015; Negro *et al.*, 2016) than those reported in human investigations. The array placement directly onto the muscle allows for a higher spatial and temporal frequency resolution and likely contributed to the relatively good performance of our EMG decomposition.

Of particular note motor unit discharge was accurately decomposed during tendon vibration with a RoA value of 92.7%. This reflexive input provides high frequency (Brown *et al.*, 1967), common input to the motoneuron pool (Mendell & Henneman, 1968) via primary muscle spindle afferents, and would be assumed to produce high levels of synchronization among motor unit discharge patterns resulting in high levels of waveform superimpositions. Consistent with the accuracy of recordings in human subjects with tremorgenic disorders (Holobar *et al.*, 2012), the high density array approach may overcome this issue as it is based on a statistical measure of sparsity, as any given motor unit discharges extremely infrequently (~10 Hz) as compared to the sampling rate, which is typically a few orders of magnitude greater (5120 Hz in this case). Intuitively, unless fully synchronized at each discharge time, the summation of two motor unit spike trains is always less sparse than the individual trains (Negro *et al.*, 2016) and the separation is possible even in case of high synchronization levels.

Though the convolutive blind source separation decomposition algorithm does not rely on traditional template matching of MUAP waveforms, reconstruction of a non-zero MUAP waveform is a necessary outcome of an accurate decomposition. If the MUAP waveforms are too similar in appearance, it is unreasonable to expect that any signal processing based decomposition approach will be able to generate valid spike times. This preparation seems ideal for this approach because the lack of non-contractile tissue under the electrodes provides less tissue filtering, preserving the higher spatiotemporal frequency content of the MUAP waveforms.

Further supporting our validation, the uniqueness of the MUAP waveform demonstrates sharp sensitivity to small amounts of noise in the spike times. Although there are a large number of non-biological solutions that can result in valid individual waveforms that are sensitive to noise (Farina *et al.*, 2014), it is highly unlikely that a set of waveforms would systematically become less different from each other when noise is added to the triggers used to extract them, unless they are generated by physiological discharges.

The reconstructed MUAP waveform also provides an opportunity to track the same motor unit across time. Waveform measurements including peak-to-peak amplitude and conduction velocity of the MUAP demonstrated some variability, but were largely stable across time. Such variability in the MUAP waveform, may have a biological origin (Farina & Falla, 2008). However, interelectrode distance, number of spikes used in the STA window, and general level of synchronization may also influence these measures. Using this tracking approach, we saw a decrease in the number of motor units matched over time. This may reflect a loss of smaller MUAP waveforms during higher levels of contractions and/or slight shifts in electrode position across contractions altering the shape of the MUAP. However, it is possible that changes in the presence of specific motor units in different contractions could also reflect changes in the distribution of synaptic drive and/or motor unit rotation (Bawa *et al.*, 2006).

Lastly, we were able to faithfully reconstruct the force output. It was expected that the summation of the spike times would accurately reproduce force generation and this was indeed the case. As discussed below, the use of motor unit spike times is superior to traditional EMG approaches.

Estimation of muscle force through electrical activity

Estimating the force generated by the muscle is important for both a comprehensive understanding of the control of human movement and the various stresses these places on the musculoskeletal system. Modeling of muscle activation using endpoint forces is limited with regards to co-contraction, whereas the interference EMG is limited by waveform cancelation (Keenan *et al.*, 2005; Keenan *et al.*, 2006; Farina *et al.*, 2008) and crosstalk (De Luca & Merletti, 1988; Farina *et al.*, 2002)

Here, we demonstrate that the rectified and filtered EMG signal provides a good estimate of the whole muscle force. Although it is possible that more advanced manipulations to the interference EMG signal might improve the accuracy of force estimates (Lloyd & Besier, 2003; Staudenmann *et al.*, 2006), our results clearly show that the CST provides superior estimates to filtered EMG. Previous investigations have utilized single motor unit discharge patterns to estimate the force generated by a muscle (Theeuwen *et al.*, 1996). Undoubtedly, the ability to control multiple parameters afforded by the discharge time of individual neurons (rate and magnitude of force generation) help the CST produce superior estimates of muscle force as compared to interference EMG. However, our current data demonstrate that individual motor unit behavior, though free from waveform cancelation and crosstalk, provided poor estimates of whole muscle force. In addition to non-linear aspects of motoneuron discharges including an initial acceleration, saturation, and hysteresis (Heckman & Enoka, 2012), the discharge patterns of individual motor units are strongly affected by synaptic noise. With the addition of a suitable number of motor unit spike trains to the CST, this noise is diminished. This allows the common components across motoneuron discharges, which the muscle force generation responds to, to be more readily observed (Farina *et al.*, 2014; Farina & Negro, 2015).

Our results however show that the improvement in force estimation from the CST versus EMG is small. There is however one important aspect of force generation where the CST is markedly superior, which is in capturing higher frequency force content. Waveform cancellation of the EMG signal limits the magnitude of variations that can be observed in the rectified and smoothed signal. The CST is immune to these effects, as waveform cancelation is not an issue once the signal is accurately decomposed. Such discrepancies may partially explain the substantial difference in the ability of the EMG and CST to estimate muscle force during the tonic discharge of motor units (correlation coefficients of 0.834 versus 0.947). Our force estimates do not yet factor in ranges of motor unit forces and we have not fully considered the non-linear properties of the muscle, including the small degree of non-arithmetic

summation of motor unit forces (Perreault *et al.*, 2003) and the significant catch-like properties (Rack & Westbury, 1969; Binder-Macleod & Clamann, 1989; Frigon *et al.*, 2011). Addition of these factors may further improve CST-based estimations of high frequency force fluctuations.

A return to parallel animal and human investigations

The discharge of individual spinal motoneurons provides a detailed window into the human motor system (reviewed in Duchateau & Enoka, 2011; Johnson *et al.*, 2017). The approach developed here allows for parallel experiments in an animal preparations and in humans. The discharge times from populations of motor units can be measured and analyzed in the same manner in both species, with the cellular mechanisms identified in the animal preparations, just as discussed above for understanding the firing patterns induced by vibration. This new parallel approach has the potential to transform our understanding of the cellular basis of motor output in both humans and animals. A recent review from the Heckman laboratory envisions this approach in detail (Johnson *et al.*, 2017). Ongoing, the insights from this parallel approach can be further enhanced by additional techniques for both animals and humans. In animals, the development of extracellular array recordings of populations of spinal interneurons (AuYong *et al.*, 2011) can further deepen the insights for cellular mechanisms. For human studies, statistical approaches for human firing data to estimate the durations of AHPs (Suresh *et al.*, 2014) and the spike triggered averaging methods to estimate twitch characteristics (Kutch *et al.*, 2010; Negro & Orizio, 2017) will also be highly advantageous. Overall, it will be important to apply these approaches in multiple muscles in the future, with the eventual goal of understanding the relationships between synaptic organization, motoneuron properties, and the diversity of the musculoskeletal system in both normal and pathological states.

Here we have quantified the neural drive to muscle in the *in vivo* cat. We have provided experimental validation using concurrent recordings from two sources, computational validation by reconstructing and corrupting the MUAP waveform within and between trials, and predictive validation by demonstrating that the CST can accurately estimate muscle force generation. This provides strong support for the validity of the underlying decomposition algorithm used in this manuscript (Holobar *et al.*, 2010). Further, these findings suggest that, while individual motor unit discharge patterns provide a poor representation of whole muscle force, an increasing number of motor units can provide superior estimates of muscle force than more traditional EMG approaches. Lastly, we have outline the preferred discharge of individual motor units in response to tendon vibration, providing a new tool to quantify reflex activation of the motor system. Understanding the discharge of partial populations of motor units will provide a

means to collect the same highly detailed signals in humans – bridging the divide between intracellular mechanisms and human motor function.

References

Adrian ED & Bronk DW. (1929). The discharge of impulses in motor nerve fibres: Part II. The frequency of discharge in reflex and voluntary contractions. *The Journal of physiology* **67,** i3-151.

AuYong N, Ollivier-Lanvin K & Lemay MA. (2011). Preferred locomotor phase of activity of lumbar interneurons during air-stepping in subchronic spinal cats. *Journal of neurophysiology* **105,** 1011-1022.

Bagust J. (1974). Relationships between motor nerve conduction velocities and motor unit contraction characteristics in a slow twitch muscle of the cat. *The Journal of physiology* **238,** 269-278.

Bawa P, Pang MY, Olesen KA & Calancie B. (2006). Rotation of motoneurons during prolonged isometric contractions in humans. *Journal of neurophysiology* **96,** 1135-1140.

Binder-Macleod SA & Clamann HP. (1989). Force output of cat motor units stimulated with trains of linearly varying frequency. *Journal of neurophysiology* **61,** 208-217.

Brown MC, Engberg I & Matthews PB. (1967). The relative sensitivity to vibration of muscle receptors of the cat. *The Journal of physiology* **192,** 773-800.

Burke RE. (1967). Motor unit types of cat triceps surae muscle. *The Journal of physiology* **193,** 141-160.

Burke RE. (1981). *Motor Units: Anatomy, Physiology, and Functional Organization*. American Physiological Society

Bethesda.

Burke RE, Levine DN, Salcman M & Tsairis P. (1974). Motor units in cat soleus muscle: physiological, histochemical and morphological characteristics. *The Journal of physiology* **238,** 503-514.

Cescon C & Gazzoni M. (2010). Short term bed-rest reduces conduction velocity of individual motor units in leg muscles. *Journal of electromyography and kinesiology : official journal of the International Society of Electrophysiological Kinesiology* **20,** 860-867.

Collins DF, Gorassini M, Bennett D, Burke D & Gandevia SC. (2002). Recent evidence for plateau potentials in human motoneurones. *Advances in experimental medicine and biology* **508,** 227-235.

De Luca CJ, LeFever RS, McCue MP & Xenakis AP. (1982). Behaviour of human motor units in different muscles during linearly varying contractions. *The Journal of physiology* **329,** 113-128.

De Luca CJ & Merletti R. (1988). Surface myoelectric signal cross-talk among muscles of the leg. *Electroencephalography and clinical neurophysiology* **69,** 568-575.

Duchateau J & Enoka RM. (2011). Human motor unit recordings: origins and insight into the integrated motor system. *Brain research* **1409,** 42-61.

Elbasiouny SM. (2014). Development of modified cable models to simulate accurate neuronal active behaviors. *J Appl Physiol (1985)* **117,** 1243-1261.

Farina D, Cescon C, Negro F & Enoka RM. (2008). Amplitude cancellation of motor-unit action potentials in the surface electromyogram can be estimated with spike-triggered averaging. *Journal of neurophysiology* **100,** 431-440.

Farina D & Falla D. (2008). Effect of muscle-fiber velocity recovery function on motor unit action potential properties in voluntary contractions. *Muscle & nerve* **37,** 650-658.

Farina D & Holobar A. (2016). Characterization of human motor units from surface EMG decomposition. *Proceedings of the IEEE* **104,** 353-373.

Farina D, Merletti R & Enoka RM. (2014). The extraction of neural strategies from the surface EMG: an update. *J Appl Physiol (1985)* **117,** 1215-1230.

Farina D, Merletti R, Indino B, Nazzaro M & Pozzo M. (2002). Surface EMG crosstalk between knee extensor muscles: experimental and model results. *Muscle & nerve* **26,** 681-695.

Farina D, Muhammad W, Fortunato E, Meste O, Merletti R & Rix H. (2001). Estimation of single motor unit conduction velocity from surface electromyogram signals detected with linear electrode arrays. *Medical & biological engineering & computing* **39,** 225-236.

Farina D & Negro F. (2015). Common synaptic input to motor neurons, motor unit synchronization, and force control. *Exercise and sport sciences reviews* **43,** 23-33.

Farina D, Negro F, Muceli S & Enoka RM. (2016). Principles of Motor Unit Physiology Evolve With Advances in Technology. *Physiology (Bethesda)* **31,** 83-94.

Frigon A, Johnson MD & Heckman CJ. (2011). Altered activation patterns by triceps surae stretch reflex pathways in acute and chronic spinal cord injury. *Journal of neurophysiology* **106,** 1669-1678.

Fuglevand AJ, Winter DA & Patla AE. (1993). Models of recruitment and rate coding organization in motor-unit pools. *Journal of neurophysiology* **70,** 2470-2488.

Gligorijevic I, Sleutjes BT, De Vos M, Blok JH, Montfoort I, Mijovic B, Signoretto M & Van Huffel S. (2015). Motor Unit Tracking Using High Density Surface Electromyography (HDsEMG) . Automated Correction of Electrode Displacement Errors. *Methods Inf Med* **54,** 221-226.

Grundy D. (2015). Principles and standards for reporting animal experiments in The Journal of Physiology and Experimental Physiology. *The Journal of physiology* **593,** 2547-2549.

Heckman CJ & Enoka RM. (2012). Motor unit. *Comprehensive Physiology* **2,** 2629-2682.

Holobar A, Glaser V, Gallego JA, Dideriksen JL & Farina D. (2012). Non-invasive characterization of motor unit behaviour in pathological tremor. *J Neural Eng* **9,** 056011.

Holobar A, Minetto MA, Botter A, Negro F & Farina D. (2010). Experimental analysis of accuracy in the identification of motor unit spike trains from high-density surface EMG. *IEEE transactions on neural systems and rehabilitation engineering : a publication of the IEEE Engineering in Medicine and Biology Society* **18,** 221-229.

Holobar A, Minetto MA & Farina D. (2014). Accurate identification of motor unit discharge patterns from high-density surface EMG and validation with a novel signal-based performance metric. *J Neural Eng* **11,** 016008.

Hu X, Rymer WZ & Suresh NL. (2013). Assessment of validity of a high-yield surface electromyogram decomposition. *Journal of neuroengineering and rehabilitation* **10,** 99.

Hu X, Rymer WZ & Suresh NL. (2014). Accuracy assessment of a surface electromyogram decomposition system in human first dorsal interosseus muscle. *J Neural Eng* **11,** 026007.

Hyngstrom A, Johnson M, Schuster J & Heckman CJ. (2008). Movement-related receptive fields of spinal motoneurones with active dendrites. *The Journal of physiology* **586,** 1581-1593.

Jankowska E, McCrea D & Mackel R. (1981). Oligosynaptic excitation of motoneurones by impulses in group Ia muscle spindle afferents in the cat. *The Journal of physiology* **316,** 411-425.

Johnson MD, Thompson CK, Tysseling VM, Powers RK & Heckman CJ. (2017). The potential for understanding the synaptic organization of human motor commands via the firing patterns of motoneurons. *Journal of neurophysiology* **118,** 520-531.

Keenan KG, Farina D, Maluf KS, Merletti R & Enoka RM. (2005). Influence of amplitude cancellation on the simulated surface electromyogram. *J Appl Physiol (1985)* **98,** 120-131.

Keenan KG, Farina D, Merletti R & Enoka RM. (2006). Amplitude cancellation reduces the size of motor unit potentials averaged from the surface EMG. *J Appl Physiol (1985)* **100,** 1928-1937.

Kutch JJ, Kuo AD & Rymer WZ. (2010). Extraction of individual muscle mechanical action from endpoint force. *Journal of neurophysiology* **103,** 3535-3546.

Lee RH & Heckman CJ. (1996). Influence of voltage-sensitive dendritic conductances on bistable firing and effective synaptic current in cat spinal motoneurons in vivo. *Journal of neurophysiology* **76,** 2107-2110.

Lee RH & Heckman CJ. (1999). Enhancement of bistability in spinal motoneurons in vivo by the noradrenergic alpha1 agonist methoxamine. *Journal of neurophysiology* **81,** 2164-2174.

Lewis DM. (1972). The effect of denervation on the mechanical and electrical responses of fast and slow mammalian twitch muscle. *The Journal of physiology* **222,** 51-75.

Lloyd DG & Besier TF. (2003). An EMG-driven musculoskeletal model to estimate muscle forces and knee joint moments in vivo. *Journal of biomechanics* **36,** 765-776.

Mambrito B & De Luca CJ. (1984). A technique for the detection, decomposition and analysis of the EMG signal. *Electroencephalography and clinical neurophysiology* **58,** 175-188.

Martinez-Valdes E, Negro F, Laine CM, Falla D, Mayer F & Farina D. (2016). Tracking motor units longitudinally across experimental sessions with high-density surface electromyography. *The Journal of physiology*.

McGill KC, Lateva ZC & Johanson ME. (2004). Validation of a computer-aided EMG decomposition method. *Conference proceedings : Annual International Conference of the IEEE Engineering in Medicine and Biology Society IEEE Engineering in Medicine and Biology Society Conference* **7,** 4744-4747.

McGill KC, Lateva ZC & Marateb HR. (2005). EMGLAB: an interactive EMG decomposition program. *Journal of neuroscience methods* **149,** 121-133.

McPherson LM, Negro F, Thompson CK, Sanchez L, Heckman CJ, Dewald J & Farina D. (2016). Properties of the motor unit action potential shape in proximal and distal muscles of the upper limb in healthy and post-stroke individuals. *Conference proceedings : Annual International Conference of the IEEE Engineering in Medicine and Biology Society IEEE Engineering in Medicine and Biology Society Conference* **2016,** 335-339.

Mendell LM & Henneman E. (1968). Terminals of single Ia fibers: distribution within a pool of 300 homonymous motor neurons. *Science* **160,** 96-98.

Muceli S, Poppendieck W, Negro F, Yoshida K, Hoffmann KP, Butler JE, Gandevia SC & Farina D. (2015). Accurate and representative decoding of the neural drive to muscles in humans with multi-channel intramuscular thin-film electrodes. *The Journal of physiology* **593,** 3789-3804.

Nawab SH, Chang SS & De Luca CJ. (2010). High-yield decomposition of surface EMG signals. *Clinical neurophysiology : official journal of the International Federation of Clinical Neurophysiology* **121,** 1602-1615.

Negro F, Muceli S, Castronovo AM, Holobar A & Farina D. (2016). Multi-channel intramuscular and surface EMG decomposition by convolutive blind source separation. *J Neural Eng* **13,** 026027.

Negro F & Orizio C. (2017). Robust estimation of average twitch contraction forces of populations of motor units in humans. *Journal of electromyography and kinesiology : official journal of the International Society of Electrophysiological Kinesiology* **37,** 132-140.

Parsaei H, Stashuk DW, Rasheed S, Farkas C & Hamilton-Wright A. (2010). Intramuscular EMG signal decomposition. *Crit Rev Biomed Eng* **38,** 435-465.

Perreault EJ, Day SJ, Hulliger M, Heckman CJ & Sandercock TG. (2003). Summation of forces from multiple motor units in the cat soleus muscle. *Journal of neurophysiology* **89,** 738-744.

Powers RK & Binder MD. (2001). Input-output functions of mammalian motoneurons. *Reviews of physiology, biochemistry and pharmacology* **143,** 137-263.

Powers RK, Elbasiouny SM, Rymer WZ & Heckman CJ. (2012). Contribution of intrinsic properties and synaptic inputs to motoneuron discharge patterns: a simulation study. *Journal of neurophysiology* **107,** 808-823.

Powers RK & Heckman CJ. (2017). Synaptic control of the shape of the motoneuron pool input-output function. *Journal of neurophysiology* **117,** 1171-1184.

Rack PM & Westbury DR. (1969). The effects of length and stimulus rate on tension in the isometric cat soleus muscle. *The Journal of physiology* **204,** 443-460.

Silverman J, Garnett NL, Giszter SF, Heckman CJ, 2nd, Kulpa-Eddy JA, Lemay MA, Perry CK & Pinter M. (2005). Decerebrate mammalian preparations: unalleviated or fully alleviated pain? A review and opinion. *Contemp Top Lab Anim Sci* **44,** 34-36.

Stashuk DW. (1999). Decomposition and quantitative analysis of clinical electromyographic signals. *Med Eng Phys* **21,** 389-404.

Staudenmann D, Kingma I, Daffertshofer A, Stegeman DF & van Dieen JH. (2006). Improving EMG-based muscle force estimation by using a high-density EMG grid and principal component analysis. *IEEE transactions on bio-medical engineering* **53,** 712-719.

Stuart DG & Brownstone RM. (2011). The beginning of intracellular recording in spinal neurons: facts, reflections, and speculations. *Brain research* **1409,** 62-92.

Suresh AK, Hu X, Powers RK, Heckman CJ, Suresh NL & Rymer WZ. (2014). Changes in motoneuron afterhyperpolarization duration in stroke survivors. *Journal of neurophysiology* **112,** 1447-1456.

Theeuwen M, Gielen CC & van Bolhuis BM. (1996). Estimating the contribution of muscles to joint torque based on motor-unit activity. *Journal of biomechanics* **29,** 881-889.

Wood SJ & Slater CR. (2001). Safety factor at the neuromuscular junction. *Progress in neurobiology* **64,** 393-429.

Yavuz US, Negro F, Sebik O, Holobar A, Frommel C, Turker KS & Farina D. (2015). Estimating reflex responses in large populations of motor units by decomposition of the high-density surface electromyogram. *The Journal of physiology* **593,** 4305-4318.

Competing Interests

The authors declare no competing interests

Author Contributions

Experiments were performed at Northwestern University. CKT, FN, DF, and CJH are responsible for the conception and design of the work. CKT, FN, MDJ, MRH, LMM, RKP, DF, and CJH are responsible for the acquisition, analysis, or interpretation of data for the work and drafting or revising the manuscript for important intellectual content. All authors have approved the final version of the manuscript and agree to be accountable for all aspects of the work. All persons designated as authors qualify for authorship, and all those who qualify for authorship are listed.

Funding

This work was supported by a Craig H. Neilsen Foundation Postdoctoral Fellowship (CKT), NIH grants T32HD007418 (CKT and MDJ), T32EB009406 (LMM), R01NS089313 (CJH) and R01NS085331 (RKP and CJH), the European Union's Horizon 2020 research and innovation programme under the Marie Skłodowska-Curie grant agreement No. 702491 (NeuralCon, FN) and by the European Research Council Advanced Grant DEMOVE (contract #267888) (DF).

Acknowledgements

We would like to thank Dr. Jack Miller for his technical assistance and insightful discussions and Ms. Rochelle O. Bright for her assistance with manuscript preparation.

Legends

Figure 1. Example EMG recording. Example of an electromyographic recording from the soleus muscle of a cat during spontaneous motor output. The signal is shown as a differential between rows resulting in a 5x12 matrix. The enlarged inset of the differentiated signal demonstrates the propagation of a single MUAP. The estimated conduction velocity of the inset motor unit is 3.3 m/s.

Figure 2. Two-source validation of the motor unit discharge times. (a) Raster plot of discharge times extracted from the fine wire recordings (color) and the array recordings (black) during the spontaneous discharge of soleus motor units. The numbers to the left indicate the average discharge rate and the coeficient of variation for each spike train. All three of the motor units detected with the fine wire recording were observed in the array recording with rate of aggreement (RoA) values ranging between 97.8 to 100%. (b) Interspike interval histograms for each motor unit are summed to compile a composite interspike interval (ISI) histogram across all units. The fine wire units are overlaid in their respective colors, with the remainder of ISIs shown in black. This composite ISI histogram demonstrates two peaks, as two of the 12 motor units are discharging at a faster discharge in the absence of any reflex input. (c) Histograms of RoA values for each of the 201 common units detected separated for each of the four modes of activation.

Figure 3. Construction of unique motor unit action potential waveforms within a trial and their sensitivity to added noise in the spike times. Motor unit action potential waveforms are constructed though spike triggered averaging the discharge times into each of the 64 channels and interpolating across the 5x13 electrode array. (a) Example of two instantaneous MUAP waveforms from the 12 soleus motor unit spike trains decomposed during a 30 s bout of tendon vibration. (b) The correlation matrices across all 12 MUAP waveforms demonstrates perfect waveform correlations with themselves (diagonal) with only 6 of the 78 incorrect pairwise MUAP waveform correlations demonstrate even moderate ($r>0.5$) correlations with other MUAP waveforms. (c) The average MUAP waveform for each of the 12 motor units demonstrates a relatively high measure of uniqueness. The derived MUAPs are sensitive just a few milliseconds of noise added to the spike times used for the STA windows. The correlation matrices shown here for 5 and 10% noise (Percent SD of ISI), reveal fewer trials with even moderate ($r>0.5$) correlations with even the same unit with different amounts of noise. With as few as 5% noise added to the spike times, the MUAP uniqueness value it significantly decreased from the no noise condition.

Figure 4. Stability of the MUAP waveform across trials. The MUAP waveforms are constructed for each active motor unit within a contraction. Units are considered the same if the 2D crosscorrelation between a MUAP in one trial and a MUAP in a different trial is >0.85. Across these 10 trials, 75% of the motor units were matched in at least 2 trials, while 3 motor units were matched across all 10 trials. Three MUAP waveforms are shown here, matched across 7, 4, and 10 trials respectively.

Figure 5. Estimation of muscle force through its electrical activity. (a) EMG (blue trace) and (b) CST (red trace) are optimized to provide the best correlation with the soleus muscle force (black trace) evoked through the crossed extension reflex. The CST produces a superior fit to the overall force profile and more accurately represents the transient decrease in force generation observed at the end of the response. (c) Across 188 trials and various modes of activation, the CST produced a better fit than five randomly chosen EMG signals. (d) The iterative addition of motor units to the CST demonstrates the discharge from a single motor unit can only produce a relatively poor correlation with force. However, with nine or motor units, the CST can produce better estimates of muscle force than the EMG estimates (grey line). Optimized EMG and CST estimates of (e) muscle force and (f) 0.75 Hz high pass muscle force of soleus evoked though crossed extension reflex. (g) Across all trials, the CST produced a better fit to the 0.75 Hz. high pass muscle than five randomly chosen EMG signals. (h) The iterative addition of motor units reveal

three or more motor units is needed to better represent the high pass muscle force than the EMG signal. In panels d and h the individual symbols represent the average correlations and refer to the primary y-axis, while the solid line represents the number of trials containing the number of units equal to or greater than those represented on the secondary y-axis.

Figure 6. Motor unit discharge in response to homonymous tendon vibration. (a) The interspike interval (ISI) histograms from ~15 motor unit spike trains in response to ~30 seconds of 130 Hz tendon vibration is shown for six different experiments. In each case, the motor unit discharge pattern consistently demonstrates a quantal discharge pattern at integer multiples of the vibration period resulting in a multimodal ISI histogram. (b) Motor unit discharge patterns from three vibration frequencies from one experiment demonstrate multimodal ISIs at the integer multiples of each of the three vibration periods. The position of tendon is shown at the inset. When motor units were tracked across trials, each motor unit demonstrates a relatively narrow preferred discharge frequency across each of the three frequencies.

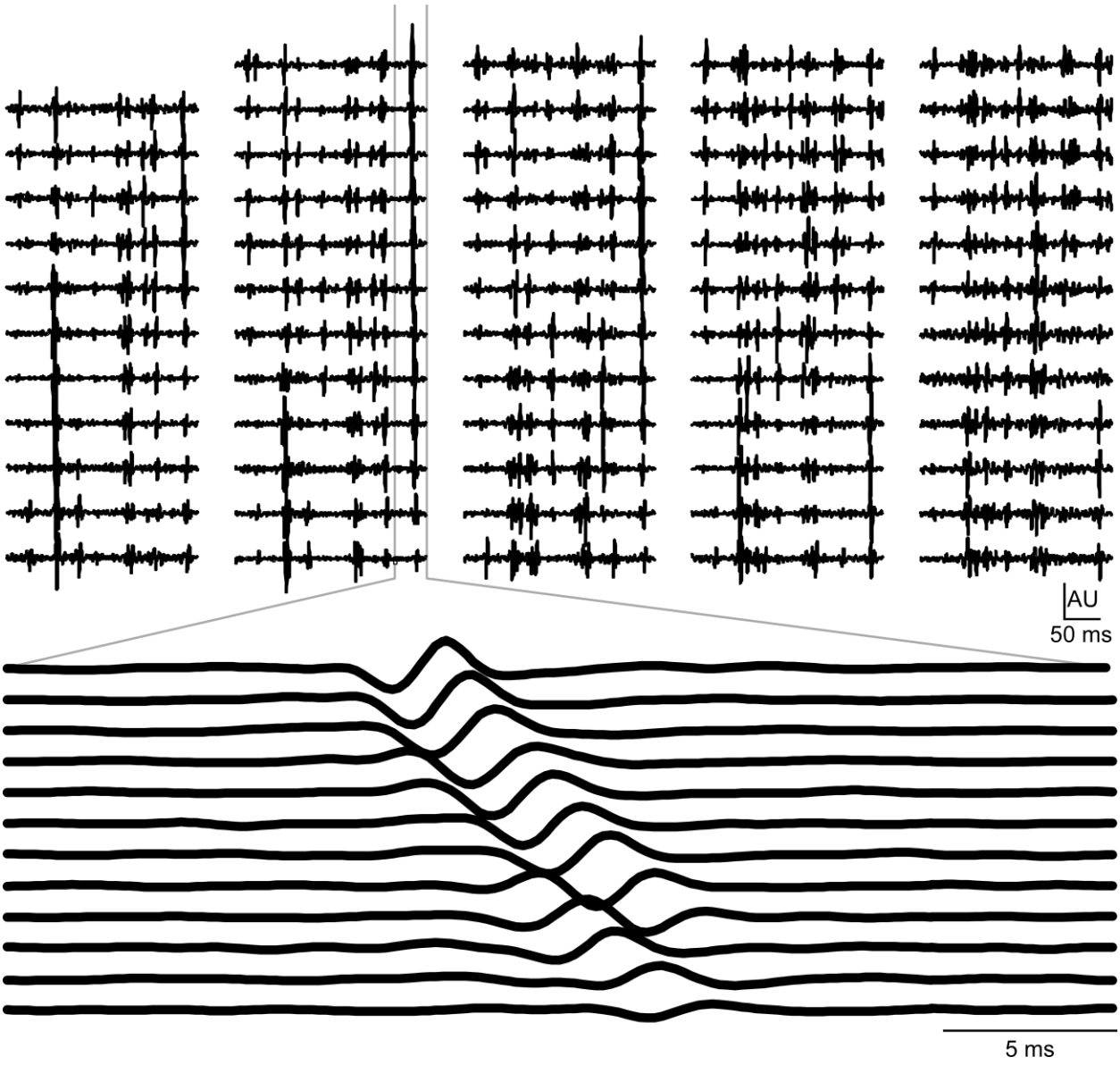

898

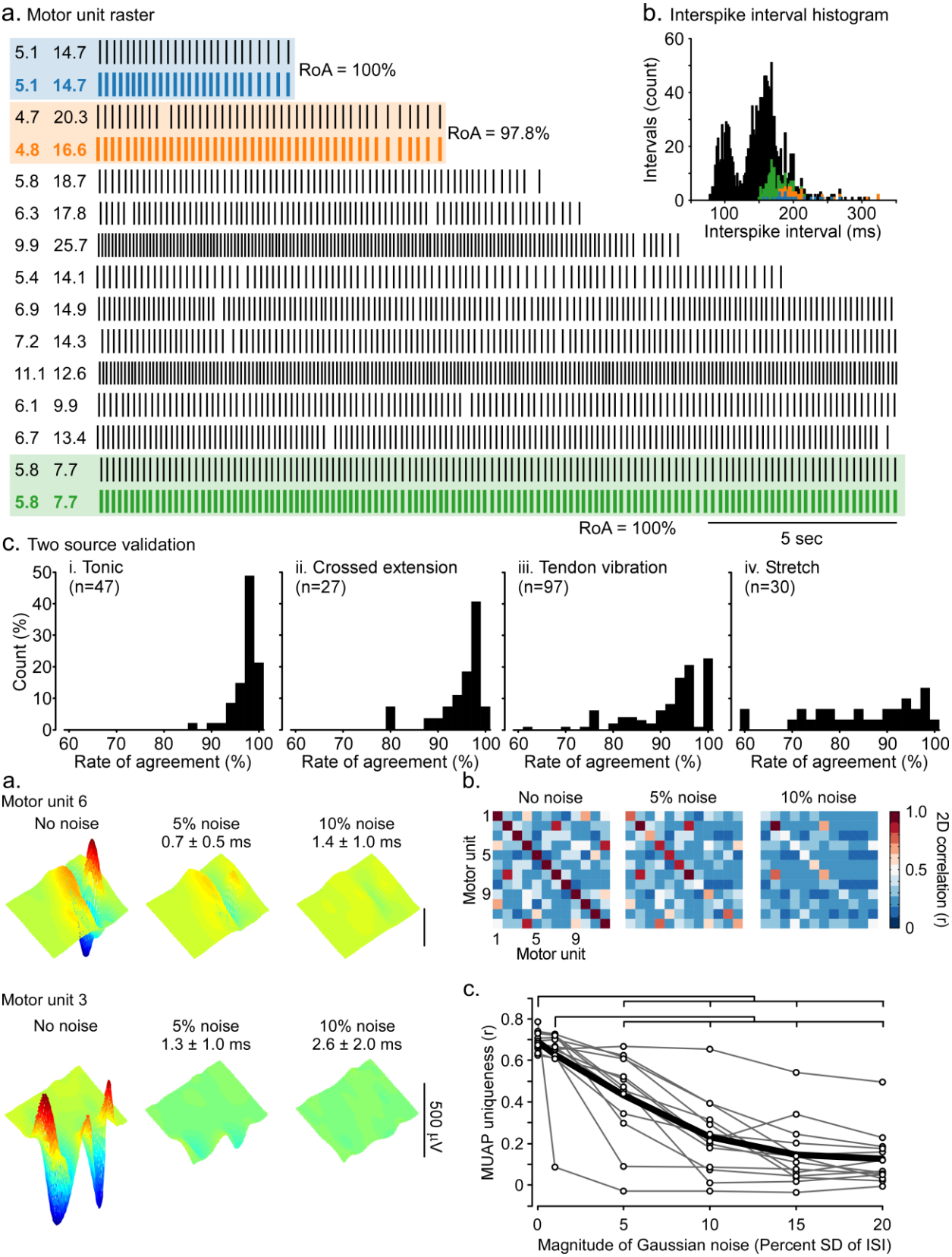
a. Motor unit raster
5.1 14.7
5.1 14.7
RoA = 100%
4.7 20.3
4.8 16.6
RoA = 97.8%
5.8 18.7
6.3 17.8
9.9 25.7
5.4 14.1
6.9 14.9
7.2 14.3
11.1 12.6
6.1 9.9
6.7 13.4
5.8 7.7
5.8 7.7
RoA = 100%
5 sec
b. Interspike interval histogram
Intervals (count)
Interspike interval (ms)
c. Two source validation
i. Tonic (n=47)
ii. Crossed extension (n=27)
iii. Tendon vibration (n=97)
iv. Stretch (n=30)
Count (%)
Rate of agreement (%)
a.
Motor unit 6
No noise
5% noise 0.7 ± 0.5 ms
10% noise 1.4 ± 1.0 ms
Motor unit 3
No noise
5% noise 1.3 ± 1.0 ms
10% noise 2.6 ± 2.0 ms
500 µV
b.
No noise
5% noise
10% noise
Motor unit
2D correlation (r)
c.
MUAP uniqueness (r)
Magnitude of Gaussian noise (Percent SD of ISI)

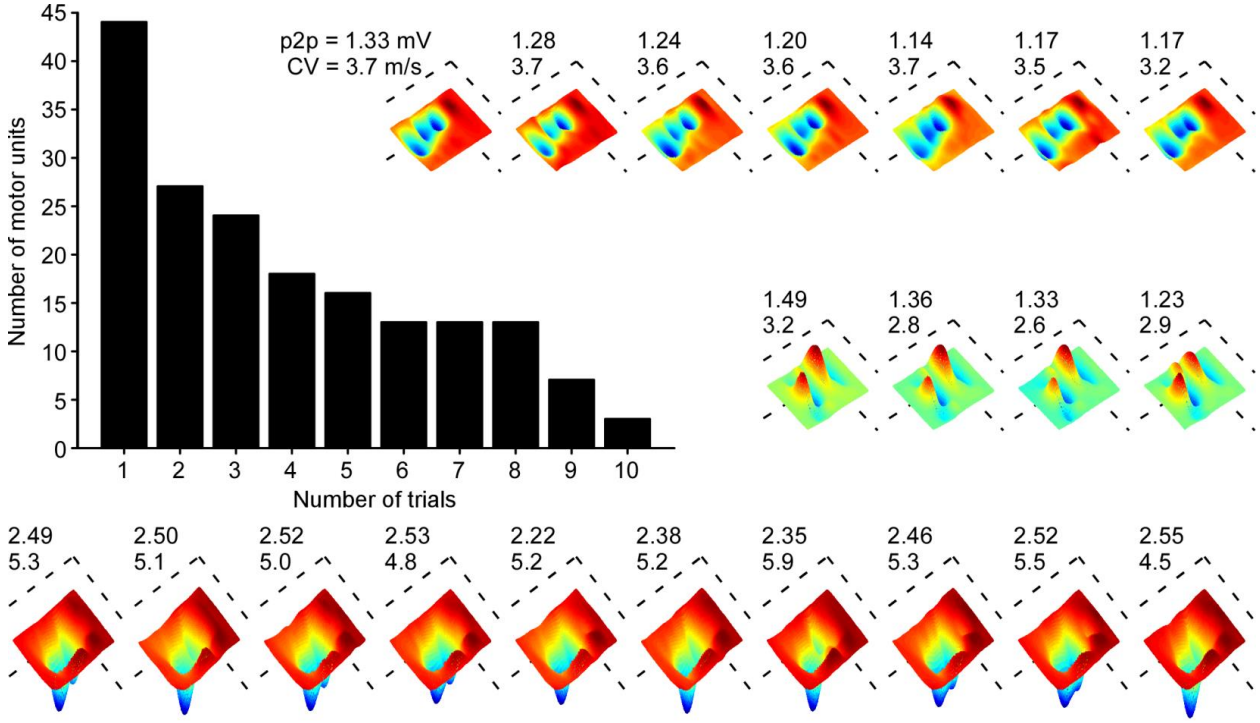
p2p = 1.33 mV
CV = 3.7 m/s
1.28
3.7
1.24
3.6
1.20
3.6
1.14
3.7
1.17
3.5
1.17
3.2
1.49
3.2
1.36
2.8
1.33
2.6
1.23
2.9
2.49
5.3
2.50
5.1
2.52
5.0
2.53
4.8
2.22
5.2
2.38
5.2
2.35
5.9
2.46
5.3
2.52
5.5
2.55
4.5
Number of motor units
0
5
10
15
20
25
30
35
40
45
1
2
3
4
5
6
7
8
9
10
Number of trials

901

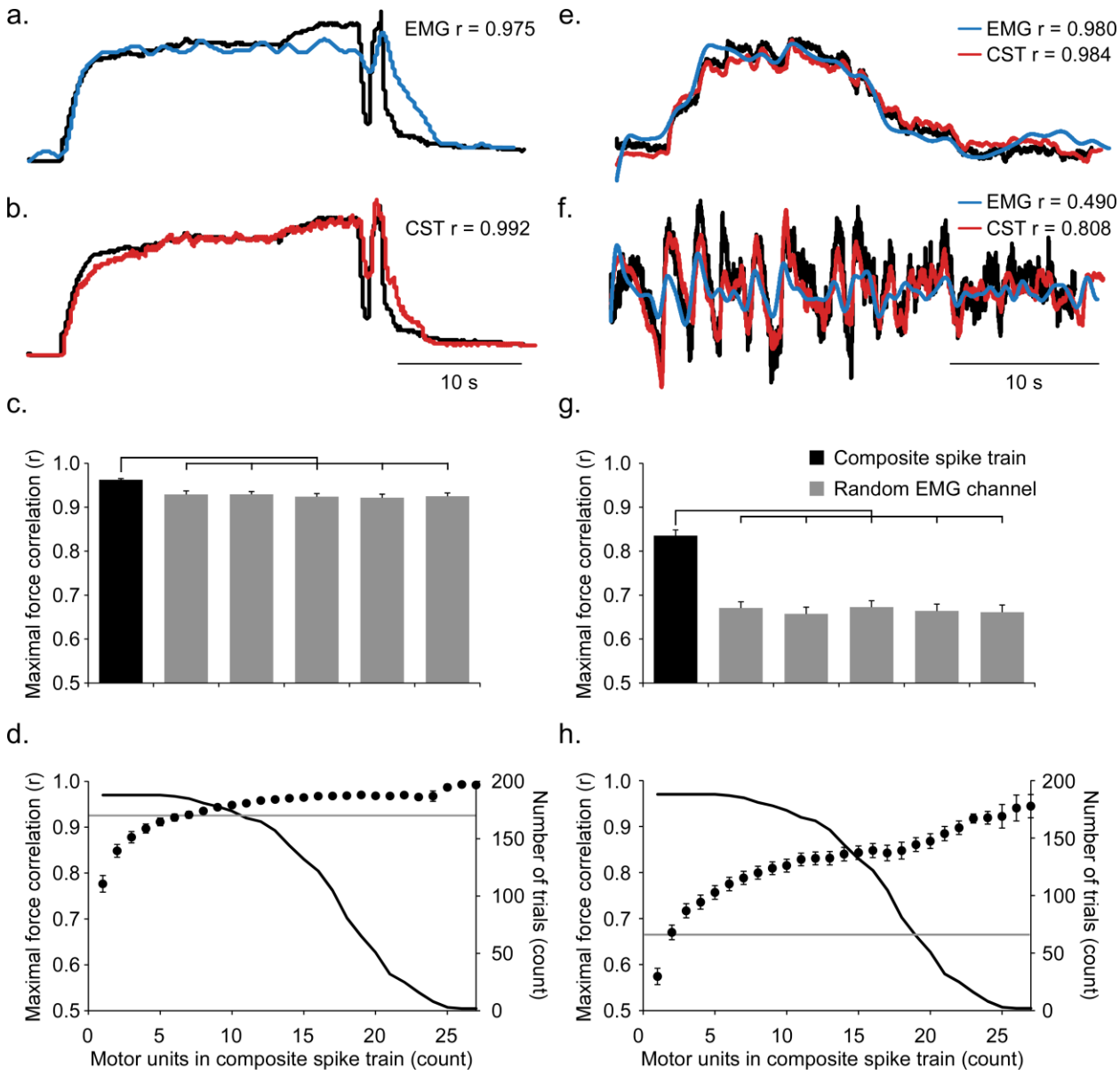
a.
EMG r = 0.975
b.
CST r = 0.992
10 s
e.
EMG r = 0.980
CST r = 0.984
f.
EMG r = 0.490
CST r = 0.808
10 s
c.
Maximal force correlation (r)
1.0
0.9
0.8
0.7
0.6
0.5
g.
Composite spike train
Random EMG channel
Maximal force correlation (r)
d.
Maximal force correlation (r)
Number of trials (count)
200
150
100
50
0
0
5
10
15
20
25
Motor units in composite spike train (count)
h.
Maximal force correlation (r)
Number of trials (count)
Motor units in composite spike train (count)

902

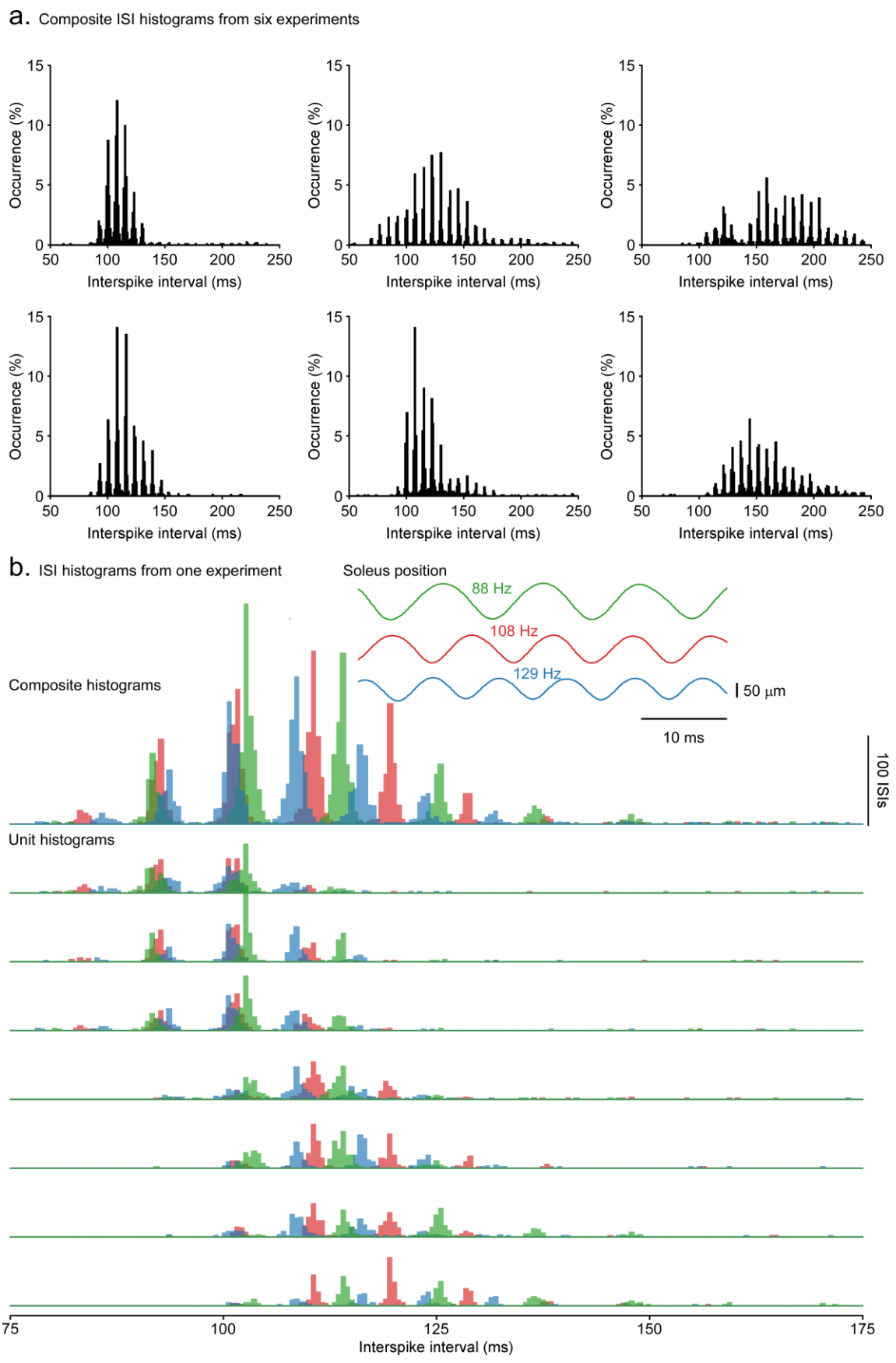
a. Composite ISI histograms from six experiments
Occurrence (%)
Interspike interval (ms)
b. ISI histograms from one experiment
Soleus position
88 Hz
108 Hz
129 Hz
50 μm
10 ms
Composite histograms
100 ISIs
Unit histograms
Interspike interval (ms)

903